# Comparison of a fluid and a solid approach for the numerical simulation of Friction Stir Welding with a non-cylindrical pin

P. Bussetta[1*], N. Dialami[2], R. Boman[1], M. Chiumenti[2],
C. Agelet de Saracibar[2], M. Cervera[2] and J-P. Ponthot[1]

[1] University of Liege, Department of Aerospace & Mechanical Engineering,
Non Linear Computational Mechanics, Building B52/3,
Chemin des Chevreuils, 1; B-4000 Liege, Belgium
e-mail: {P.Bussetta; R.Boman; JP.Ponthot}@ulg.ac.be

[2] International Centre for Numerical Methods in Engineering (CIMNE)
Universidad Politécnica de Cataluña
Campus Norte UPC, 08034 Barcelona, Spain
e-mail: {narges; michele; agelet; cervera}@cimne.upc.edu

## Abstract

Friction Stir Welding (FSW) process is a solid-state joining process during which materials to be joined are not melted. As a consequence, the heat-affected zone is smaller and the quality of the weld is better with respect to more classical welding processes. Because of extremely high strains in the neighbourhood of the tool, classical numerical simulation techniques have to be extended in order to track the correct material deformations. The Arbitrary Lagrangian Eulerian (ALE) formulation is used to preserve a good mesh quality throughout the computation. With this formulation the mesh displacement is independent from the material displacement. Moreover, some advanced numerical techniques such as remeshing or a special computation of transition interface is needed to take into account non-cylindrical tools. During the FSW process, the behaviour of the material in the neighbourhood of the tool is at the interface between solid mechanics and fluid mechanics. Consequently, a numerical model of the FSW process based on a solid formulation is compared to another one based on a fluid formulation. It is shown that these two formulations essentially deliver the same results in terms of pressures and temperatures.

**Keywords:** Friction Stir Welding (FSW), Finite Element Method, Remeshing, Arbitrary Lagrangian Eulerian (ALE) formalism

# 1   Introduction and state of the art in FSW

Friction Stir Welding (FSW) is a new method of welding in solid state, created and patented by The Welding Institute (TWI) in 1991 [1]. In FSW a cylindrical, shouldered tool with a profiled probe, also called pin, is rotated and slowly plunged into the joint line between two

pieces of sheet or plate material, which are butted together. The parts have to be clamped onto a backing bar in a manner that prevents the abutting joint faces from being forced apart. Once the probe has been completely inserted, it is moved with a small tilt angle in the welding direction. The shoulder applies a pressure on the material to constrain the plasticised material around the probe tool. Due to the advancing and rotating effect of the probe and shoulder of the tool along the seam, an advancing side and a retreating side are formed and the softened and heated material flows around the probe to its backside where the material is consolidated to create a high-quality solid-state weld (see figure 1). The maximum temperature reached is of the order of 80% of the melting temperature. Despite the simplicity of the procedure, the mechanisms behind the process and the material flow around the probe tool are very complex. The material is extruded around the rotating tool and a vortex flow field near the probe due to the downward flow is induced by the probe thread. The process can be regarded as a solid phase keyhole welding technique since a hole to accommodate the probe is generated, then filled during the welding sequence. The material flow depends on welding process parameters, such as welding and rotation speed, pressure, etc., and on the characteristics of the tools, such as materials, design, etc.


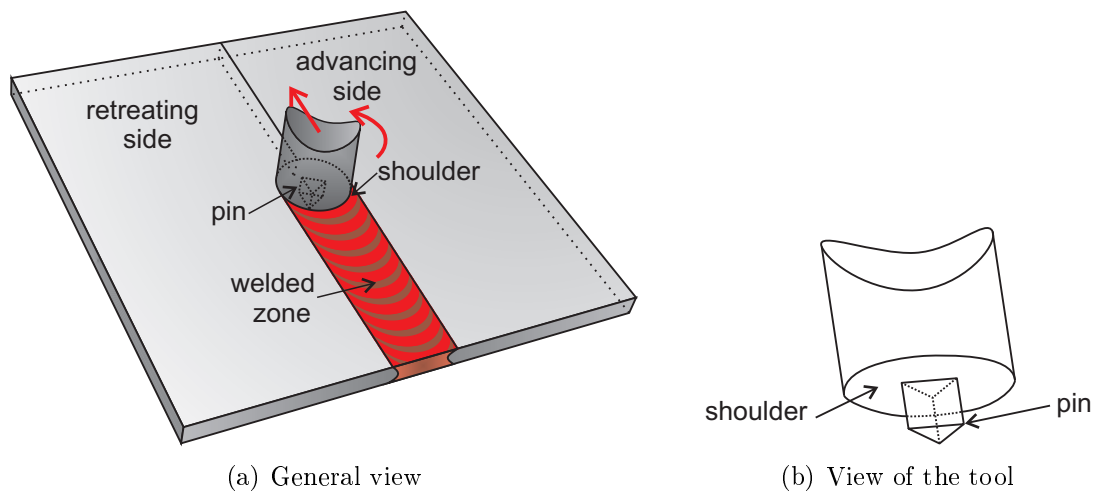
(a) General view      (b) View of the tool

Figure 1: Scheme of the FSW process.

The first applications of FSW have been in aluminium fabrications. Aluminium alloys that are difficult to weld using conventional welding techniques, are successfully welded using FSW. The weld quality is excellent, with none of the porosity that can arise in fusion welding, and the mechanical properties are at least as good as the best achievable by fusion welding. Being a solid-state welding process, the structure in the weld nugget is free of solidifying segregation, being suitable for welding of composite materials. The process is environmentally friendly, because no fumes or spatter are generated, and there is no arc glare or reflected laser beams with which to contend. Another major advantage is that, by avoiding the creation of a molten pool which shrinks significantly on re-solidification, the distortion after welding and the residual stresses are low. With regard to joint fit up, the process can accommodate a gap of up to 10% of the material thickness without impairing the quality of the resulting weld. As far as the rate of processing is concerned, for materials of 2 mm thickness, welding speeds of up to 2 m/min can be achieved, and for 5 mm thickness up to 0.75 m/min. Recent tool

developments are confidently expected to improve on these figures.

Friction stir welding has been used to weld all wrought aluminium alloys, across the AA-2xxx, AA-5xxx, AA-6xxx and AA-7xxx series of alloys, some of which are bordering on being classed as virtually unweldable by fusion welding techniques. The process can also weld dissimilar aluminium alloys, whereas fusion welding may result in the alloying elements from the different alloys interacting to form deleterious intermetallics through precipitation during solidification from the molten weld pool. Friction stir welding can also make hybrid components by joining dissimilar materials such as aluminium and magnesium alloys. The thicknesses of AA-6082-T6 that have so far been welded have ranged from 1.2 mm to 50 mm in a single pass, to more than 75 mm when welding from both sides. Welds have also been made in pressure die cast aluminium material without any problems from pockets of entrapped high pressure gas, which would violently disrupt a molten weld pool encountering them.

The original application for friction stir welding was the welding of long lengths of material in the aerospace, shipbuilding and railway industries. Examples include large fuel tanks and other containers for space launch vehicles, cargo decks for high-speed ferries, and roofs for railway carriages. FSW is used already in routine, as well as in critical applications, for the joining of structural components made of aluminium and its alloys. Indeed, it has been convincingly demonstrated that the process results in strong and ductile joints, sometimes in systems which have proved difficult using conventional welding techniques. The process is most suitable for components which are flat and long (plates and sheets) but can be adapted for pipes, hollow sections and positional welding.

The computational modelling of FSW processes is a complex task and it has been a research topic of increasing interest in computational mechanics during the last decades.

Thermal models for the numerical simulation of FSW processes were used by McClure et al. (1998) [2], Colegrove et al. (2000) [3], and Khandkar and Khan (2001,2003) [4, 5].

Bendzsak et al. (2000) [6, 7] used the Eulerian code Stir3D to model the flow around a FSW tool, including the tool thread and tilt angle in the tool geometry and obtaining complex flow patterns. The temperature effects on the viscosity were neglected.

Dong et al. (2001) [8] developed a simplified model for the numerical simulation of FSW processes, taking into account both the friction heating and plastic work in the modelling of the heat flow phenomena, predicting the development of a plastic strain around the weld zone in the initial stage of welding. However, they did not consider the longitudinal movement of the tool.

Xu et al. (2001) [9] and Xu and Deng (2003) [10] developed a 3D finite element procedure to simulate the FSW process using the commercial Finite Element Method (FEM) software ABAQUS, focusing on the velocity field, the material flow characteristics and the equivalent plastic strain distribution. The authors used an Arbitrary Lagrangian-Eulerian (ALE) formulation with adaptive meshing and consider large elasto-plastic deformations and temperature-dependent material properties. However, the authors did not perform a fully coupled thermo-mechanical simulation, superimposing the temperature map obtained from the experiments as a prescribed temperature field to perform the mechanical analysis. The numerical results were compared to experimental data available, showing a reasonable good correlation between the equivalent plastic strain distributions and the distribution of the microstructure zones in the weld.

Ulysse (2002) [11] presented a fully coupled 3D FEM visco-plastic model for FSW of thick aluminium plates using the commercial FEM code FIDAP. The author investigated the effect of tool speeds on the process parameters. It was found that a higher translational speed leads to a higher welding force, while increasing the rotation speed has the opposite effect.

Reasonable agreement between the predicted and the measured temperature was obtained and the discrepancies were explained by an inadequate representation of the constitutive behaviour of the material for the wide ranges of strain-rate, temperatures and strains typically found during FSW.

Askari et al. (2003) [12] used the CTH hydrocode coupled to an advection-diffusion solver for the energy balance equation. The CTH code, developed by Sandia National Laboratories, uses the finite volume method to discretize the domain. The elastic response was taken into account in this case. The results proved encouraging with respect to gaining an understanding of the material flow around the tool. However, simplified friction conditions were used.

Chen and Kovacevic (2003) [13] developed a 3D FEM model to study the thermal history and thermo-mechanical phenomena in the butt-welding of aluminium alloy AA-6061-T6 using the commercial FEM code ANSYS. Their model incorporated the mechanical reaction between the tool and the weld material. Experiments were conducted and an X-ray diffraction technique was used to measure the residual stress in the welded plate. The welding tool (i.e. the shoulder and pin) in the FEM model was modeled as a heat source, with the nodes moved forward at each computational time step. This simple model severely limited the accuracy of the stress and force predictions.

Colegrove et al. (2000, 2004) [3, 14] used the commercial Computational Fluid Dynamics (CFD) software FLUENT for a 2D and 3D numerical investigation on the influence of pin geometry during FSW, comparing different pin shapes in terms of material flow and welding forces on the basis of both a stick and a slip boundary condition at the tool/work-piece interface. In spite of the good obtained results, the accuracy of the analysis was limited by the assumption of isothermal conditions. Seidel and Reynolds (2003) [15] also used the CFD commercial software FLUENT to model the 2D steady-state flow around a cylindrical tool.

Schmidt and Hattel (2004) [16] presented the development of a 3D fully coupled thermo-mechanical finite element model in ABAQUS/Explicit using the ALE formulation. The flexibility of the FSW machine was taken into account by connecting the rigid tool to a spring. The work-piece was modelled as a cylindrical volume with inlet and outlet boundary conditions. A rigid back-plate was used. The contact forces were modelled using a Coulomb friction law, and the surface was allowed to separate. Heat generated by friction and plastic deformation was considered. The simulation modelled the dwell and weld phases of the process.

An ALE formulation for the numerical simulation of FSW processes was also used by Zhao (2005) [17], by Guerdoux (2007) [18] and Assidi et al. (2010) [19].

Nikiforakis (2005) [20] used a finite difference method to model the FSW process. Despite the fact that he was only presenting 2D results, the model proposed had the advantage of minimizing the calibration of model parameters, taking into account a maximum of physical effects. A transient and fully coupled thermo-fluid analysis was performed. The rotation of the tool was handled through the use of the overlapping grid method. A rigid-viscoplastic material law was used and sticking contact at the tool work piece interface was assumed. Hence, heating was due to plastic deformation only.

Heurtier et al. (2006) [21] used a 3D semi-analytical coupled thermomechanical FE model to simulate FSW processes. The model uses an analytical velocity field and considers heat input from the tool shoulder and plastic strain of the bulk material. Trajectories, temperature, strain, strain rate fields and micro-hardness in various weld zones were computed and compared to experimental results obtained on an AA 2024-T351 alloy FSW joint.

Buffa et al. (2006) [22] using the commercial finite element software DEFORM-3D, proposed a 3D Lagrangian, implicit, coupled thermo-mechanical numerical model for the simulation of FSW processes, using a rigid-viscoplastic material description and a continuum assumption for the weld seam. The proposed model is able to predict the effect of process

parameters on process variables, such as the temperature, strain and strain rate fields, as well as material flow and forces. A reasonable good agreement between the numerically predicted results, on forces and temperature distribution, and experimental data was obtained. The authors found that the temperature distribution about the weld line is nearly symmetric because the heat generation during FSW is dominated by rotating speed of the tool, which is much higher than the advancing speed. On the other hand, the material flow in the weld zone is non-symmetrically distributed about the weld line because the material flow during FSW is mainly controlled by both advancing and rotating speeds.

De Vuyst et al. (2004-2006) [23, 24, 25, 26] used the coupled thermo-mechanical finite element code MORFEO to simulate the flow around simplified tool geometries for FSW process. The rotation and advancing speed of the tool were modelled using prescribed velocity fields. An attempt to consider features associated to the geometrical details of the probe and shoulder, which had not been discretized in the finite element model in order to avoid very large meshes, was taken into account using additional special velocity boundary conditions. In spite of that, a mesh of roughly 250,000 nodes and almost 1.5 million of linear tetrahedral elements was used. A Norton-Hoff rigid-viscoplastic constitutive equation was considered, with averaged values of the consistency and strain rate sensitivity constitutive parameters determined from hot torsion tests performed over a range of temperatures and strain rates. The computed streamlines were compared with the flow visualization experimental results obtained using copper marker material sheets inserted transversally or longitudinally to the weld line. The simulation results correlated well when compared to markers inserted transversely to the welding direction. However, when compared to a marker inserted along the weld centreline only qualitative results could be obtained. The correlation may be improved by modelling the effective weld thickness of the experiment, using a more realistic material model, for example, by incorporating a yield stress or temperature dependent properties, refine velocity boundary conditions or further refining the mesh in specific zones, such as for instance, under the probe. The authors concluded that it is essential to take into account the effects of the probe thread and shoulder thread in order to get realistic flow fields.

Shercliff et al. (2005) [27] developed microstructural models for friction stir welding of 2000 series aluminium alloys.

López et al. (2008) [28] and Agelet de Saracibar et al. (2013) [29] developed numerical algorithms to optimize material model and FSW process parameters using neural networks. They proposed a new model for the dissolution of precipitates in fully hardened aluminium alloys and they optimized the master curve and the effective activation energy. Furthermore, they developed an algorithm to optimize the advancing and rotation speed, taking as weld quality criteria the minimization of the maximum hardness drop at the transversal section under the pin.

Santiago et al. (2010) [30] developed a simplified computational model taking into account the real geometry of the tool, i.e. the probe thread, and using an ALE formulation. They considered also a simplified friction model to take into account different slip/stick conditions at the pin shoulder/work-piece interface.

Agelet de Saracibar et al. (2010) [31, 32], Agelet de Saracibar et al. (2011) [33], Chiumenti et al. (2013) [34], and Dialami et al. (2013) [35] used a sub-grid scale finite element stabilized mixed velocity/pressure/ temperature formulation for coupled thermo-rigid-plastic models, using Eulerian and Arbitrary Lagrangian Eulerian (ALE) formalisms, for the numerical simulation of Friction Stir Welding (FSW) processes. They used ASGS and OSGS methods and quasi-static sub-grid scales, neglecting the sub-grid scale pressure and using the finite element component of the velocity in the convective term of the energy balance equation.

Chiumenti et al. (2013) [34], Dialami et al. (2013) [35], and Chiumenti et al. (2013) [36]

developed an apropos kinematic framework for the numerical simulation of FSW processes. They considered a combination of ALE, Eulerian and Lagrangian descriptions at different zones of the computational domain and they proposed an efficient coupling strategy. Within this approach, a Lagrangian formulation was used for the pin, an ALE formulation was used at the stir zone of the work-piece, and an Eulerian formulation was used in the remaining part of the work-piece. The stir zone was defined as a circular domain close to the pin. The finite element mesh in the stir zone was rotating attached to the pin. The resulting apropos kinematic setting efficiently permitted to treat arbitrary pin geometries and facilitates the application of boundary conditions. The formulation was implemented in an enhanced version of the finite element code COMET [37] developed by the authors at the International Centre for Numerical Methods in Engineering (CIMNE).

Chiumenti et al. (2013) [36] used a novel stress-accurate FE technology for highly non-linear analysis with incompressibility constraints typically found in the numerical simulation of FSW processes. They used a mixed linear piece-wise interpolation for displacement, pressure and stress fields, respectively, resulting in an enhanced stress field approximation which enables for stress accurate results in nonlinear computational mechanics.

This paper presents and compares two different numerical models of the FSW process, in the general case of a non-cylindrical pin. The first model is based on a solid approach written in terms of nodal positions and nodal temperatures. The second model of FSW process is based on a fluid approach written in terms of the velocity, the pressure and the temperature fields. Both models use advanced numerical techniques such as remeshing and the ALE formulation.

# 2   2D Numerical modelling of FSW process

The FSW process is modelled in two dimensions under the plane strain hypothesis. To model this welding process, the displacement of the tool is split into an advancing movement (actually assigned to the work-pieces but, in the opposite direction) and a rotation (imposed to the tool).

In other words, the centre of the pin is fixed and a constant velocity is imposed to the plates (see figure 2(a)). The tool is described by a classical Lagrangian mesh. Then, in relation with the distance to the centre of the tool, three zones of the plates are identified. In the closest zone around the pin, the material is submitted to extremely high strains. This region is called the *thermo-mechanically affected zone* (TMAZ). Due to high deformations, the use of a Lagrangian formalism would lead very quickly to mesh entanglement. Thus, in this region, the ALE formulation is employed. On top of this, the ALE formulation allows the model to take into account non-circular pin shapes. In this zone, the mesh has the same rotational speed as the pin (red region in figure 2(b)). In the furthest zone from the tool, the grey zone in figure 2(b), the Eulerian formulation is used. Thus in this region, the mesh is fixed. The ring connecting region 1 and region 3 is a transition zone (white region numbered 2 in figure 2(b)). In such a model, the quality of the mesh does not change during the simulation except in the transition zone. So, to overcome this problem, two different numerical techniques are proposed (see section 2.2.2).
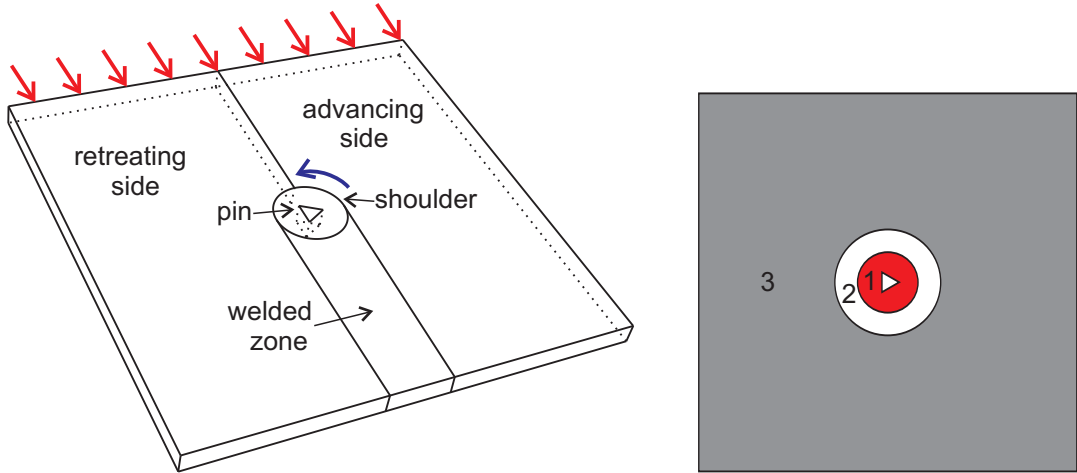
(a) Scheme of the FSW model. A rotation is imposed to the pin (blue arrow) while the advancing velocity of the pin is replaced by a velocity imposed to the plates in the opposite direction (red arrows).

(b) The different zones of the model: ALE formulation is used on the red region (1), the transition zone corresponds to the white region (2), and the Eulerian formulation is applied on the grey region (3)

Figure 2: Description of the FSW model

## 2.1 Thermomechanical formulation

The numerical models presented here are based on the finite element method. In this paper, two numerical formulations are compared. The first one is based on a solid mechanics approach. It is written in terms of nodal positions and temperatures. The second one is based on a fluid mechanics approach. The equilibrium is written as a function of nodal velocities, pressures and temperatures.

**Solid approach** In the solid approach, the finite element used are linear quadrilaterals. The position and temperature fields are computed at each node of the elements. The stresses and the internal variables are computed at each quadrature point of the element (4 Gauss points). To overcome the locking phenomenon, the pressure is considered constant over the element and computed only at a central quadrature point. The thermomechanical equations are split into a mechanical part and a thermal part. At each time step, the mechanical equations are first solved using a constant temperature field. This temperature field is the one obtained at the latest increment. Then, the thermal equations are solved on the frozen resulting geometrical configuration that has just been obtained.

**Fluid approach** The fluid approach is based on a stabilized mixed linear temperature-velocity-pressure finite element formulation. This formulation is stabilized adopting the Orthogonal Sub-Grid Scale method (OSS) [38, 39, 40] to solve both the pressure instability induced by the incompressibility constraint and the instabilities coming from the convective term. A triangular mesh is used for the domain discretization. The velocity, the pressure and

temperature fields are computed at each node of the element. The deviatoric stresses and the other internal variables are computed at each quadrature point of the element. Finally, the coupled thermo-mechanical problem is solved by means of a staggered time-marching scheme where the thermal and mechanical sub-problems are solved sequentially, within the framework of the classical fractional step methods [41, 42]. This approach is exposed in more detail in [35, 34, 38, 40].

## 2.2 Numerical simulation strategy

### 2.2.1 Arbitrary Lagrangian Eulerian formulation

In region 1 and region 3 in figure 2(b) the ALE formulation is used. Indeed, the Eulerian formulation (used in the region 3) is a particular case of the ALE formulation. In the ALE formalism, unlike in the Lagrangian case which is commonly used in Solid Mechanics, the mesh no longer follows the material motion [35, 34, 43, 44, 45]. Consequently, a new grid coordinate system $R_{\vec{\chi}}$ is defined and the conservation laws able to describe the FSW process are rewritten in terms of the new coordinates $\vec{\chi}$:

Mass:
$$\left.\frac{\partial \rho}{\partial t}\right|_{\vec{\chi}} + \vec{c}.\vec{\nabla}\rho + \rho\vec{\nabla}.\vec{v} = 0 \tag{1}$$

Momentum:
$$\rho\left(\left.\frac{\partial \vec{v}}{\partial t}\right|_{\vec{\chi}} + (\vec{c}.\vec{\nabla})\vec{v}\right) = \vec{\nabla}.\boldsymbol{\sigma} + \rho\vec{b} \tag{2}$$

Energy:
$$\rho C_p\left(\left.\frac{\partial T}{\partial t}\right|_{\vec{\chi}} + \vec{c}.\vec{\nabla}T\right) = D_{mech} - \vec{\nabla}.\vec{q} \tag{3}$$

where $\rho$ and $C_p$ are the mass density and the specific heat capacity, $\boldsymbol{\sigma}$ is the Cauchy stress tensor, $\vec{b}$ is the specific body forces, $T$ is the temperature, $D_{mech}$ is the plastic dissipation rate per unit of volume. The heat flux, $\vec{q}$, is defined according to the isotropic Fourier's law as:

$$\vec{q} = -k\vec{\nabla}T \tag{4}$$

The convective velocity $\vec{c} = \vec{v} - \vec{v^*}$ is the difference between the material velocity $\vec{v}$ and the mesh velocity $\vec{v^*}$. Both the stress tensor, $\boldsymbol{\sigma}$, and the strain rate tensor, $\boldsymbol{D}$, are split into volumetric and deviatoric parts:

$$\boldsymbol{\sigma} = p\boldsymbol{I} + \boldsymbol{S} \tag{5}$$

$$\boldsymbol{D} = \frac{1}{3}D_{vol}\boldsymbol{I} + \widehat{\boldsymbol{D}} \tag{6}$$

where $p$ and $\boldsymbol{S}$ are the pressure and the stress deviator, respectively. Similarly, $D_{vol} = tr(\boldsymbol{D})$ and $\widehat{\boldsymbol{D}} = dev(\boldsymbol{D})$ are the volumetric and the deviatoric parts of the strain-rate tensor, respectively.

The thermal boundary conditions are defined in terms of the heat flux that flows through the boundaries by heat convection and radiation. They are expressed by Newton and radiation laws, respectively, as:

$$q_{conv} = h_{conv}(T - T_{env}) \tag{7}$$

$$q_{rad} = \sigma_0\varepsilon(T^4 - T_{env}^4) \tag{8}$$

where $h_{conv}$ is the heat transfer coefficient by convection, $\sigma_0$ is the Stefan-Boltzmann constant and $\varepsilon$ is the emissivity factor. Finally, $T_{env}$ is the surrounding environment temperature.

The ALE formulations used in the two approaches are different.

**Solid approach**   The ALE formulation used in the solid approach is described in more details in [43, 44, 45]. To simplify the solution procedure and remain competitive against Lagrangian models, the system of ALE equations (equations 1 to 3) is solved using an operator-split procedure. First, for each time step, the classical Lagrangian thermomechanically coupled formalism is used. During this Lagrangian step the mesh sticks to the material ($\vec{\boldsymbol{v}^*} = \vec{\boldsymbol{v}}, \vec{\boldsymbol{c}} = \vec{\boldsymbol{0}}$) until an equilibrated Lagrangian configuration is iteratively obtained. So, the weak form of the governing equations which are solved during this first step is defined over the current integration domain $\Omega$ and its boundary $\partial\Omega$ (see equations 9 and 10). Let us assume that the boundary $\partial\Omega$ can be split into $\partial\Omega_\sigma$ and $\partial\Omega_u$, being $\partial\Omega = \partial\Omega_\sigma \cup \partial\Omega_u$ such that tractions are prescribed on $\partial\Omega_\sigma$ while displacements are specified on $\partial\Omega_u$, respectively. In a similar way, boundary $\partial\Omega$ can be also split into $\partial\Omega_q$ and $\partial\Omega_\theta$ such that $\partial\Omega = \partial\Omega_q \cup \partial\Omega_\theta$, where fluxes (on $\partial\Omega_q$) and temperatures (on $\partial\Omega_\theta$) are prescribed for the heat transfer analysis.

$$\int_\Omega \left( \rho \frac{d^2 \vec{\boldsymbol{u}}}{dt^2}.\delta\vec{\boldsymbol{u}} \right) dV = \int_\Omega (\rho\vec{\boldsymbol{b}}.\delta\vec{\boldsymbol{u}})dV - \int_\Omega (\boldsymbol{\sigma} : \vec{\boldsymbol{\nabla}}\delta\vec{\boldsymbol{u}})dV + \int_{\partial\Omega_\sigma} (\vec{\boldsymbol{t}}.\delta\vec{\boldsymbol{u}})dS \tag{9}$$

$$\int_\Omega \left( \rho C_p \frac{dT}{dt}\delta T \right) dV + \int_\Omega [k\vec{\boldsymbol{\nabla}}T.\vec{\boldsymbol{\nabla}}(\delta T)]dV = \int_\Omega (D_{mech}\delta T) dV - \int_{\partial\Omega_q} [(q_{conv} + q_{rad})\delta T]dS \tag{10}$$

where $\delta\vec{\boldsymbol{u}}$ and $\delta T$ are the test functions of the displacement and temperature fields. $\vec{\boldsymbol{t}}$ is prescribed tractions on the boundary domain $\partial\Omega_\sigma$.

The second step, also called the Eulerian step, is divided into two substeps: first the nodes of the mesh are relocated to a more suitable position, thus defining a new mesh with the same topology and the mesh velocity $\vec{\boldsymbol{v}^*}$. In the case of region 1 and region 3 the position of the relocated nodes is known because the mesh velocity of these regions is imposed. Then, the unknowns and the internal variables are transferred from the old mesh to the new one [45].

**Fluid approach**   The ALE formulation used in the fluid model is not based on a operator-split like in the formulation presented for the solid approach. In this fully coupled formulation [35, 34], the equilibrium state is computed at each time increment without remeshing and remapping steps. The system of equations solved includes the convective terms due to the velocity of the mesh relative to the material. In the TMAZ, region 1 in figure 2(b), the velocity of the mesh is imposed and the velocity and the pressure of the material are directly computed. In the case of the Eulerian formulation (region 3 in figure 2(b)), the mesh does not move during the computation. The following assumptions are considered for the numerical simulation of the FSW process (more detail can be found in [35, 34]):

- The flow is assumed to be incompressible as the volumetric changes including thermal deformation are found to be negligible, $D_{vol} = \vec{\boldsymbol{\nabla}}.\vec{\boldsymbol{v}} \cong 0$.

- Therefore, the deviatoric part of total strain rate tensor, $\widehat{\boldsymbol{D}}$, is computed as the symmetric part of the velocity gradient as: $\widehat{\boldsymbol{D}} = dev(\dot{\boldsymbol{\varepsilon}}) = \vec{\boldsymbol{\nabla}}^s \vec{\boldsymbol{v}}$.

- Due to the very high viscosity of the material, the material flow is characterized by very low values of Reynolds number (Re≪1). This is the reason why, in the balance of momentum equation, the inertia term can be neglected.

The governing equations which are used to describe the thermo-mechanical problem able to describe the FSW process are: the mass conservation (equation 1), the balance of momentum equation (equation 2) and the balance of energy equation (equation 3). Taking into account the previous assumptions, these governing equations can be rewritten:
Mass:

$$\vec{\boldsymbol{\nabla}}.\vec{\boldsymbol{v}} = 0 \tag{11}$$

Momentum:

$$\vec{\boldsymbol{\nabla}}.\boldsymbol{S} + \vec{\boldsymbol{\nabla}}p + \rho\vec{\boldsymbol{b}} = 0 \tag{12}$$

Energy:

$$\rho C_p \left( \left. \frac{\partial T}{\partial t} \right|_{\vec{\chi}} + \vec{\boldsymbol{c}}.\vec{\boldsymbol{\nabla}}T \right) = D_{mech} - \vec{\boldsymbol{\nabla}}.\vec{\boldsymbol{q}} \tag{13}$$

The weak form of these equations is defined over the integration domain $\Omega$ and its boundary $\partial\Omega$ (see equations 14, 15 and 18). Let us assume that the boundary $\partial\Omega$ can be split into $\partial\Omega_\sigma$ and $\partial\Omega_v$, being $\partial\Omega = \partial\Omega_\sigma \cup \partial\Omega_v$ such that tractions are prescribed on $\partial\Omega_\sigma$ while velocities are specified on $\partial\Omega_v$, respectively. In a similar way, boundary $\partial\Omega$ can be also split into $\partial\Omega_q$ and $\partial\Omega_\theta$ such that $\partial\Omega = \partial\Omega_q \cup \partial\Omega_\theta$, where fluxes (on $\partial\Omega_q$) and temperatures (on $\partial\Omega_\theta$) are prescribed for the heat transfer analysis.

$$\int_\Omega \left[ (\vec{\boldsymbol{\nabla}}.\vec{\boldsymbol{v}})\delta p \right] dV = 0 \tag{14}$$

$$\int_\Omega (\boldsymbol{S} : \vec{\boldsymbol{\nabla}}^s \delta\vec{\boldsymbol{v}}) dV + \int_\Omega (p\vec{\boldsymbol{\nabla}}.\delta\vec{\boldsymbol{v}}) dV = W_{mech} \tag{15}$$

$$\int_\Omega \left( \rho C_p \left[ \left. \frac{\partial T}{\partial t} \right|_{\vec{\chi}} + \vec{\boldsymbol{c}}.\vec{\boldsymbol{\nabla}}T \right] \delta T \right) dV + \int_\Omega [k\vec{\boldsymbol{\nabla}}T.\vec{\boldsymbol{\nabla}}(\delta T)] dV = W_{ther} \tag{16}$$

where $\delta\vec{\boldsymbol{v}}$, $\delta p$ and $\delta T$ are the test functions of the velocity, pressure and temperature fields, respectively while the mechanical and the thermal work are defined as:

$$W_{mech} = \int_\Omega (\rho\vec{\boldsymbol{b}}.\delta\vec{\boldsymbol{v}}) dV + \int_{\partial\Omega_\sigma} (\vec{\boldsymbol{t}}.\delta\vec{\boldsymbol{v}}) dS \tag{17}$$

$$W_{ther} = \int_\Omega (D_{mech}\delta T) dV - \int_{\partial\Omega_q} [(q_{conv} + q_{rad})\delta T] dS \tag{18}$$

where $\vec{\boldsymbol{t}}$ is prescribed tractions on the boundary domain $\partial\Omega_\sigma$.

### 2.2.2  The transition zone

**Solid approach**  In the solid approach, the transition zone is a ring with a finite thickness (region 2 in figure 2(b)). In this region, the evolution of the rotational speed of the mesh, which differs from the material velocity, is linearly interpolated between the ALE region and the Eulerian zone. As the mesh distortion grows with time, a remeshing operation is periodically required. For one full rotation of the pin, the remeshing process is applied 30 times. The time interval between two successive remeshings is thus constant.

The remeshing operation can be divided into two steps. First, a better-suited mesh, called the new mesh, is created. In the case of the transition zone, the relatively simple geometry of this region allows an easy generation of the new quadrangular mesh.

Then, to carry on the computation over this mesh, the state variables from the mesh before remeshing, called the old mesh, has to be transferred to the new one. Each field used to define the equilibrium state is transferred independently from the other ones. The data transfer method used in this paper is called the Finite Volume Transfer Method (FVTM) with linear reconstruction of the fields. In [46, 47], this transfer method is presented in more details and the comparison with some of the remapping algorithms most commonly used in the literature brings to light the advantages of this method.

**Fluid approach**  In the fluid model the transition zone (region 2 in figure 2(b)) is limited to a circle (zero thickness). Each node of the mesh on this circle is duplicated. One node is linked to the ALE region (numbered 1) and the other one to the Eulerian region (numbered 3). The coupling between both regions is performed using a specific node-to-node link approach. At every mesh movement step, for a given node of the ALE region, the corresponding node of the Eulerian one is found and a link between the two nodes is created. Afterwards, the boundary conditions and the properties of the plate nodes are copied to the corresponding TMAZ nodes within the link. The time step can be conveniently chosen such that the two interface meshes (ALE and Eulerian) are always compatible. In this case the ALE mesh would slide precisely from one Eulerian interface node to the next one at each time step.

### 2.2.3  Thermomechanical constitutive model

In both models, the constitutive model of the tool is thermo-rigid. So, no mechanical fields are computed over this material. However, from the point of view of the thermal equations, the tool has a classical thermal behaviour as far as heat conduction is concerned. In addition, the material behaviour of the plates is modelled as thermo-visco-plastic using a Norton-Hoff constitutive model:

$$\boldsymbol{S} = 2\mu(T)\widehat{\boldsymbol{D}}\left(\sqrt{3}\sqrt{\frac{2}{3}\widehat{\boldsymbol{D}}:\widehat{\boldsymbol{D}}}\right)^{m(T)-1} \tag{19}$$

where $m$ and $\mu$ are the rate sensitivity and viscosity parameters respectively. Both are temperature dependent.

In the FSW process, the heat is mostly generated by the mechanical dissipation, which is computed as a function of the plastic strain rate and the deviatoric stresses as:

$$D_{mech} = \gamma \boldsymbol{S} : \widehat{\boldsymbol{D}} \tag{20}$$

where $\gamma \approx 0.9$ is the fraction of the total plastic energy converted into heat.

**Solid approach**  In the solid model, the value of the variation of the pressure ($dp$) is computed thanks to the variation of the volume ($dV$) and the bulk modulus ($K$): $dp = KdV$. In addition, with the solid approach, it is possible to replace the Norton-Hoff constitutive model with a thermo-elasto-visco-plastic one, see e.g. [48]. With this kind of constitutive model, it is possible to compute the residual stresses.

**Fluid approach**  In the fluid model, the material is assumed to be incompressible and this constraint is incorporated into the equations to be solved.

### 2.2.4 Thermomechanical contact

**Solid approach**  In the solid model, a perfect sticking thermomechanical contact is considered between the tool and the work-piece. It means that the temperature field and the displacement field are continuous through the interface between the tool and the work-piece.

**Fluid approach**  The heat flux is also produced by the friction between pin and the work-piece. This heat flux can be expressed using the Norton's friction model. The heat generated by friction is split into a part absorbed by the pin (noted $q_{frict}^{pin}$) and another one absorbed by the work-piece (noted $q_{frict}^{SZ}$):

$$q_{frict}^{pin} = \vartheta^{pin}(\vec{\boldsymbol{t}}_T.\Delta\vec{\boldsymbol{v}}_T) = \vartheta^{pin}a(T)\,\|\Delta\vec{\boldsymbol{v}}_T\|^{q+1} \tag{21}$$

$$q_{frict}^{SZ} = \vartheta^{SZ}(\vec{\boldsymbol{t}}_T.\Delta\vec{\boldsymbol{v}}_T) = \vartheta^{SZ}a(T)\,\|\Delta\vec{\boldsymbol{v}}_T\|^{q+1} \tag{22}$$

where the amount of heat absorbed by the pin, $\vartheta^{pin}$, and by the work-piece, $\vartheta^{SZ}$, depends on the thermal diffusivity, $\alpha = \frac{k}{\rho C_p}$, of the two materials in contact as:

$$\vartheta^{pin} = \frac{\alpha^{pin}}{\alpha^{pin} + \alpha^{SZ}} \tag{23}$$

$$\vartheta^{SZ} = \frac{\alpha^{SZ}}{\alpha^{pin} + \alpha^{SZ}} \tag{24}$$

The tangential component of the traction vector at the contact interface, $\vec{\boldsymbol{t}}_T$, is defined as:

$$\vec{\boldsymbol{t}}_T = a(T)\,\|\Delta\vec{\boldsymbol{v}}_T\|^q \vec{\boldsymbol{u}}_T \tag{25}$$

where $a(T)$ is the (temperature dependent) material consistency, $0 \leq q \leq 1$ is the strain rate sensitivity and $\vec{\boldsymbol{u}}_T = \frac{\Delta\vec{\boldsymbol{v}}_T}{\|\Delta\vec{\boldsymbol{v}}_T\|}$ is the tangential unit vector, defined in terms of the relative tangential velocity at the contact interface, $\vec{\boldsymbol{v}}_T$.

# 3  Comparison of numerical results based on the two approaches

In this paper, the numerical results of the solid approach are compared with the already validated model based on the fluid approach (see [30, 34, 35, 49]). In this example, the section of the pin is an equilateral triangle (figures 3 and 4(a)). The mesh used with the solid model is presented at the beginning of the computation in figure 3. The dimensions of the tool are:

- radius of the circumscribed circle to the pin: 3 *mm*.

The width of the two plates is 50 *mm* and the simulated length is 100 *mm*. The simulated region of the plates is a square with a side of 100 *mm*. The centre of the pin is on the centre of this square (see figures 3 and 4(a)).
The most important parameters of the considered FSW process are:

- rotation speed: 40 *RPM*

- welding speed: 400 *mm min*$^{-1}$.

The thermo-mechanical properties of the plates are the following:

- density: 2700 *kg m*$^{-3}$

- bulk modulus: 69 $GPa$ (used only with the solid approach)
- thermo-mechanical Norton-Hoff law (presented in the part 2.2.3)
  with $\mu = 100\ MPa$, $m = 0.12$,
- heat conductivity: 120 $W\ m^{-1}\ K^{-1}$
- thermal expansion coefficient: $1 \times 10^{-6}\ K^{-1}$
- heat capacity: 875 $J\ kg^{-1}\ K^{-1}$

The thermo-mechanical properties of the tool are the following:

- density: 7800 $kg\ m^{-3}$;
- heat conductivity: 43 $W\ m^{-1}\ K^{-1}$;
- heat capacity: 460 $J\ kg^{-1}\ K^{-1}$.

The total time of the simulation is 15 seconds which corresponds to 10 revolutions for the pin.
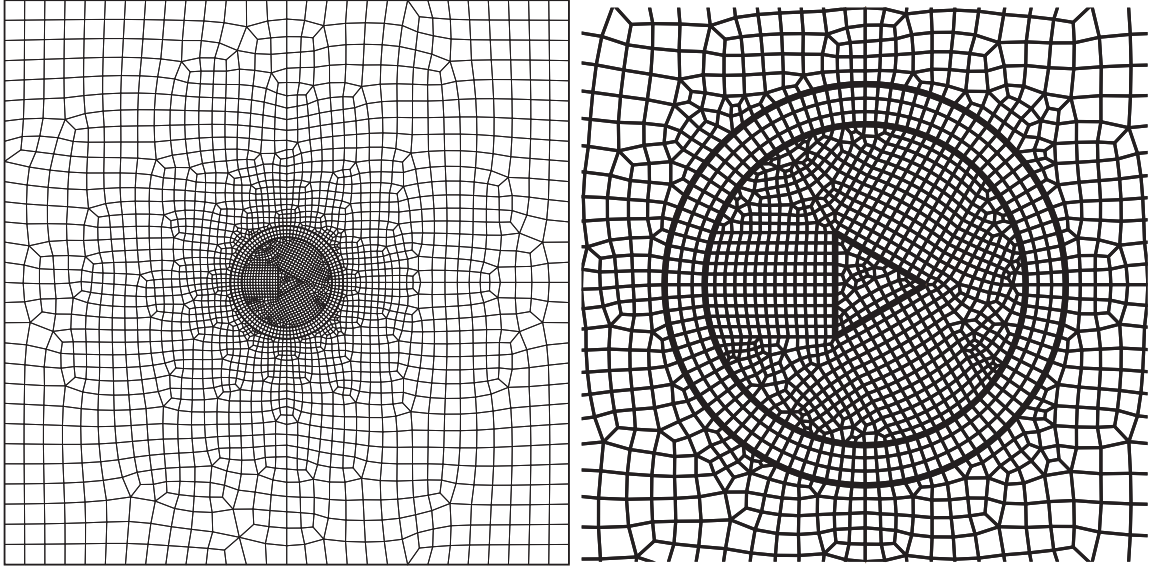


Figure 3: Initial quadrangular mesh (composed of 3237 elements) used in the solid model (global view and zoom)

Figures 4(b), 4(c) and 4(d) show the evolution of the pressure computed by the two models at three reference points defined in figure 4(a). Points 1 and 2 move with the mesh, because these points have the same rotational speed as the pin. On the other hand, point 3 is fixed in space. Figure 5 presents the evolution of the temperature computed with the two models at the three reference points. After a transient phase which depends on the numerical strategy adopted for each approach, the results of both models are very similar (see figures 4 and 5). The difference of frequency between the pressure at point 3 and the pressure and the temperature at points 1 and 2 is explained by the fact that point 3 is fixed in space while points 1 and 2 have the same rotational velocity as the pin. On the one hand, the pressure at point 3 is affected by the three corners of the pin. On the other hand, the frequency of the pressure and the temperature at points 1 and 2 are controlled by the rotation speed of the pin.

(a) The different zones of the model with the initial position of three selected points

(b) Pressure at point 1 (rotating with the pin)

(c) Pressure at point 2 (rotating with the pin)

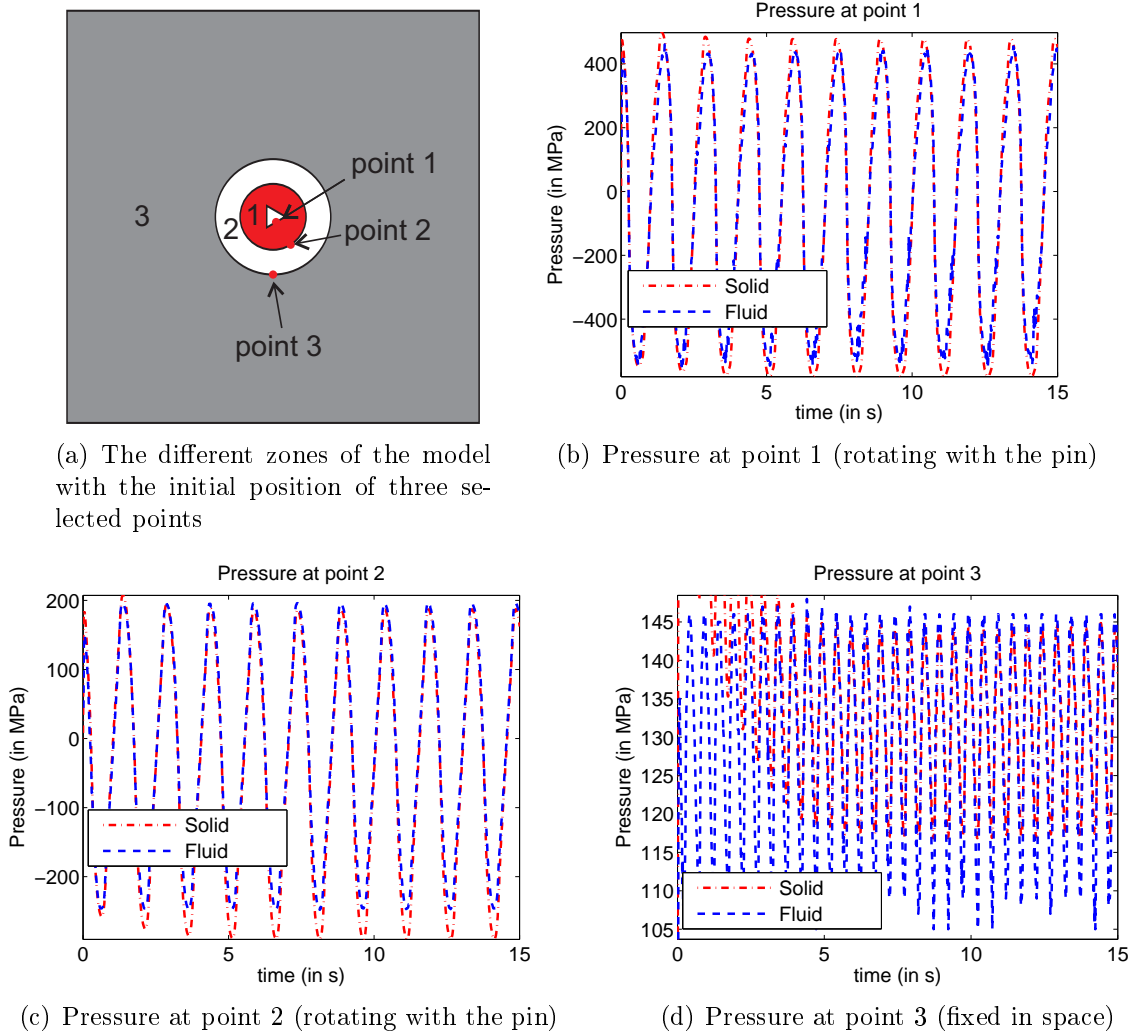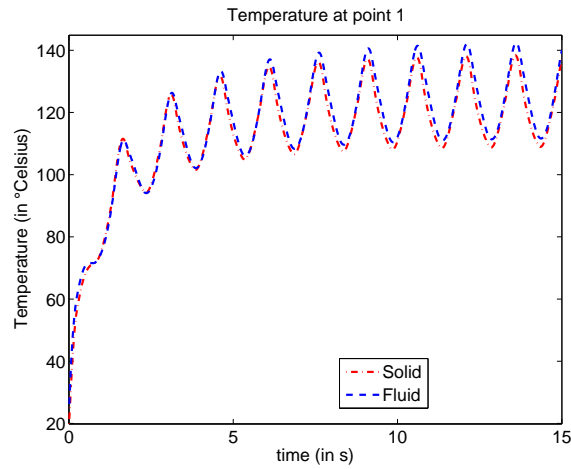(d) Pressure at point 3 (fixed in space)

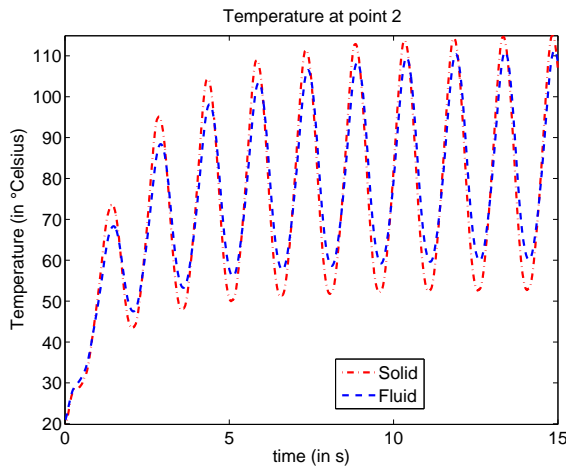Figure 4: Evolution of the pressure computed by the two models at the three reference points

Consequently, the frequency of the pressure at point 3 is three times higher than the frequency of the pressure or the temperature at points 1 or 2. Figure 6 presents the temperature field at the end of the simulation with the solid model.

# 4   Conclusion and future works

The phenomena happening during the Friction Stir Welding (FSW) process are at the interface between solid mechanics and fluid mechanics. In this paper, two different methods are presented to simulate the FSW process numerically. One model is based on a solid approach which computes the position and the temperature fields and another one is based on a fluid approach written in terms of velocity, pressure and temperature fields. Both models use advanced numerical techniques such as the Arbitrary Lagrangian Eulerian formalism or remeshing operations or an advanced stabilization algorithm. These advanced numerical techniques allow the simulation of the FSW process with non-circular tool shapes. The aim of the paper was to compare two computational models based respectively on solid and fluid

(a) Temperature at point 1 (rotating with the pin)



(b) Temperature at point 2 (rotating with the pin)
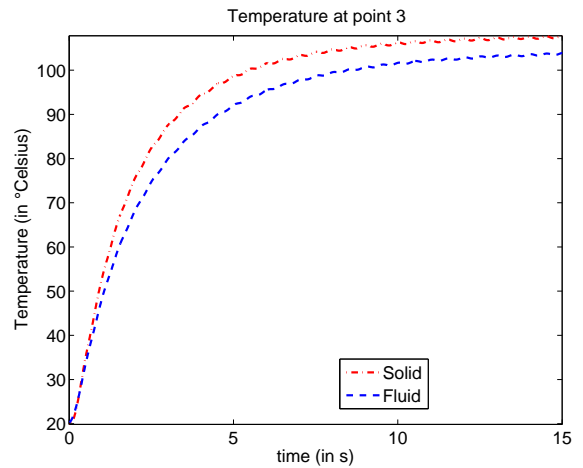
(c) Temperature at point 3 (fixed in space)

Figure 5: Evolution of the temperature computed by the two models at the three reference points

approach for the solution of FSW process. Based on the authors' point of view, being able to simulate a process using a solid model and at the same time a fluid model, is numerically very interesting and represents a further verification of the implementation in both approaches. The presented example (with a triangular pin) shows that the two formulations essentially deliver the same results. More investigations are still needed to understand the small differences between the two models. While the fluid model is more efficient from a computational point of view, the model based on the solid approach has the advantage that it can be used to compute the residual stresses (the thermo-visco-plastic constitutive model can be replaced with a thermo-elasto-visco-plastic one).
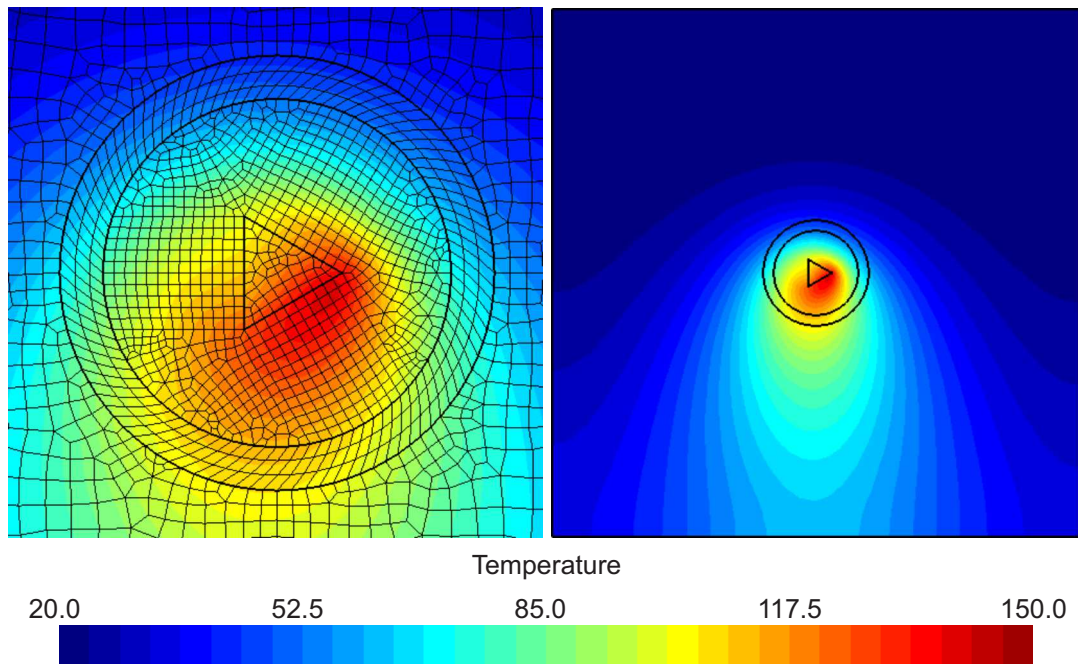
## Acknowledgements

15

Figure 6: Temperature field (in °C) at the end of the computation (time : 15 s) obtained with the solid model

# References

[1] W.M. Thomas, E.D. Nicholas, J.C. Needham, M.G. Murch, P. Temple-Smith, and C.J. Dawes. Friction stir butt welding. GB Patent No. 9125978.8, International Patent No. PCT/GB92/02203, 1991.

[2] J.C. McClure, W. Tang, L.E. Murr, X. Guo, Z. Feng, and J.E. Gould. A thermal model of friction stir welding. In *Proceedings of the 5th International Conference on Trends in Welding Research*, pages 590 − 595, Pine Mountain, Georgia, USA, June 1 - 5 1998.

[3] P. Colegrove, M. Painter, D. Graham, and T. Miller. Three dimensional flow and thermal modelling of the friction stir welding process. In *Proceedings of the 2nd International Symposium on Friction Stir Welding (2ISFSW)*, Gothenburg, Sweden, June 27 - 29 2000.

[4] M. Khandkar and J. Khan. Thermal modeling of overlap friction stir welding for Al-alloys. *Journal of Materials Processing and Manufacturing Science*, 10:91 −105, 2001. doi: 10.1177/1062065602010002613.

[5] M. Khandkar, J. Khan, and A. Reynolds. Prediction of temperature distribution and thermal history during friction stir welding: input torque based model. *Science and Technology of Welding and Joining*, 8(3):165 −174, 2003. doi: 10.1179/136217103225010943.

[6] G. Bendzsak, T. North, and C. Smith. An experimentally validated 3D model for friction stir welding. In *Proceedings of the 2nd International Symposium on Friction Stir Welding (2ISFSW)*, Gothenburg, Sweden, June 27 - 29 2000.

[7] G. Bendzsak, T. North, and C. Smith. Material properties relevant to 3-D fsw modeling. In *Proceedings of the 2nd International Symposium on Friction Stir Welding (2ISFSW)*, Gothenburg, Sweden, June 27 - 29 2000.

[8] P. Dong, F. Lu, J.K. Hong, and Z. Cao. Coupled thermomechanical analysis of friction stir welding process using simplified models. *Science and Technology of Welding and Joining*, 6(5):281 − 287, 2001. doi: 10.1179/136217101101538884.

[9] S. Xu, X. Deng, A.P. Reynolds, and T.U. Seidel. Finite element simulation of material flow in friction stir welding. *Science and Technology of Welding and Joining*, 6(3):191 −193, 2001. doi: 10.1179/136217101101538640.

[10] S. Xu and X. Deng. Two and three-dimensional finite element models for the friction stir welding process. In *Proceedings of the 4th International Symposium on Friction Stir Welding (4ISFSW)*, Park City, Utah, USA, May 14 - 16 2003.

[11] P. Ulysse. Three-dimensional modeling of the friction stir-welding process. *International Journal of Machine Tools and Manufacture*, 42:1549 − 1557, 2002. doi: 10.1016/S0890-6955(02)00114-1.

[12] A. Askari, S. Silling, B. London, and M. Mahoney. Modeling and analysis of friction stir welding processes. In *Proceedings of the 4th International Symposium on Friction Stir Welding (4ISFSW), GKSS Workshop*, Park City, Utah, USA, May 14 - 16 2003.

[13] C.M. Chen and R. Kovacevic. Finite element modeling of friction stir welding - thermal and thermomechanical analysis. *International Journal of Machine Tools and Manufacture*, 43(13):1319 − 1326, 2003. doi: 10.1016/S0890-6955(03)00158-5.

[14] P. Colegrove, H. Shercliff, and P. Threadgill. Modelling the friction stir welding of aerospace alloys. In *Proceedings of the 5th International Symposium on Friction Stir Welding (5ISFSW)*, Metz, France, September 14-16 2004.

[15] T.U. Seidel and A.P. Reynolds. Two-dimensional friction stir welding process model based on fluid mechanics. *Science and Technology of Welding and Joining*, 8(3):175 − 183, 2003. doi: 10.1179/136217103225010952.

[16] H. Schmidt and J. Hattel. Modelling thermo mechanical conditions at the tool/matrix interface in friction stir welding. In *Proceedings of the 5th International Symposium on Friction Stir Welding (5ISFSW)*, Metz, France, September 14-16 2004.

[17] H. Zhao. *Friction Stir Welding (FSW) simulation using an Arbitrary Lagrangian-Eulerian (ALE) moving mesh approach.* PhD thesis, West Virginia University, Morgantown, West Virginia, USA, 2005. URL http://hdl.handle.net/10450/4367.

[18] S. Guerdoux. *Numerical Simulation of the Friction Stir Welding Process.* PhD thesis, Ecole Nationale Supérieure des Mines de Paris, 2007.

[19] M. Assidi, L. Fourment, S. Guerdoux, and T. Nelson. Friction model for friction stir welding process simulation: Calibrations from welding experiments. *International Journal of Machine Tools and Manufacture*, 50(2):143–155, 2010. doi: 10.1016/j.ijmachtools.2009.11.008.

[20] N. Nikiforakis. Towards a whole system simulation of fsw. In *Proceedings of the 2nd FSW Modelling and Flow Visualisation Seminar*, GKSS Forschungszentrum, Geesthacht, Germany, January 31 - February 1 2005.

[21] P. Heurtier, M.J. Jones, C. Desrayaud, J.H. Driver, F. Montheillet, and D. Allehaux. Mechanical and thermal modeling of friction stir welding. *Journal of Materials Processing Technology*, 171(3):348 – 357, 2006. doi: 10.1016/j.jmatprotec.2005.07.014.

[22] G. Buffa, J. Hua, R. Shivpuri, and L. Fratini. A continuum-based fem model for friction stir welding – model development. *Materials Science and Engineering: A*, 419(1-2):389 – 396, 2006. doi: 10.1016/j.msea.2005.09.040.

[23] T. De Vuyst, L. D'Alvise, A. Simar, B. de Meester, and S. Pierret. Finite element modelling of friction stir welding aluminium alloys plates – inverse analysis using a genetic algorithm. *Welding in the World*, 49(3/4):44 – 55, 2005.

[24] T. De Vuyst, L. D'Alvise, A. Simar, B. de Meester, and S. Pierret. Inverse analysis using a genetic algorithm for the finite element modelling of friction stir welding. In *Proceedings of the 5th International Symposium on Friction Stir Welding (5ISFSW)*, Metz, France, September 14-16 2004.

[25] T. De Vuyst, L. D'Alvise, A. Robineau, and J.C. Goussain. Material flow around a friction stir welding tool – experiment and simulation. In *Proceedings of the 8th International Seminar on Numerical Analysis of Weldability*, Graz, Austria, September 25 - 27 2006.

[26] T. De Vuyst, L. D'Alvise, A. Robineau, and J.C. Goussain. Simulation of the material flow around a friction stir welding tool. In *Proceedings of the 6th International Symposium on Friction Stir Welding (6ISFSW)*, Saint-Sauveur, Quebec, Canada, October 10 - 13 2006.

[27] H.R. Shercliff, M.J. Russell, A. Taylor, and T.L. Dickerson. Microstructural modeling in friction stir welding of 2000 series aluminium alloys. *Mécanique & Industries*, 6(1):25 – 35, 2005. doi: 10.1051/meca:2005004.

[28] R. López, B. Ducoeur, M. Chiumenti, B. de Meester, and C. Agelet de Saracibar. Modeling precipitate dissolution in hardened aluminium alloys using neural networks. *International Journal of Material Forming*, 1:1291 – 1294, 2008. doi: 10.1007/s12289-008-0139-4.

[29] C. Agelet de Saracibar, R. López, B. Ducoeur, M. Chiumenti, and B. de Meester. Un modelo numérico para la simulación de disolución de precipitados en aleaciones de aluminio con endurecimiento utilizando redes neuronales. *Revista Internacional de Métodos Numéricos para Cálculo y Diseño en la Ingeniería*, 29:29 – 37, 2013. doi: 10.1016/j.rimni.2012.02.003.

[30] D. Santiago, G. Lombera, S. Urquiza, C. Agelet de Saracibar, and M. Chiumenti. Modelado termo-mecánico del proceso de friction stir welding utilizando la geometría real de la herramienta. *Revista Internacional de Métodos Numéricos para Cálculo y Diseño en Ingeniería*, 26:293 – 303, 2010.

[31] C. Agelet de Saracibar, M. Chiumenti, D. Santiago, N. Dialami, and G. Lombera. On the numerical modeling of fsw processes. In *Proceedings of the International Symposium on Plasticity and its Current Applications, Plasticity 2010*, St. Kitts, St. Kitts and Nevis, January 3 - 8 2010.

[32] C. Agelet de Saracibar, M. Chiumenti, D. Santiago, M. Cervera, N. Dialami, and G. Lombera. A computational model for the numerical simulation of fsw processes. In *Proceedings of the 10th International Conference on Numerical Methods in Industrial Forming Processes*, volume 1252, pages 81 – 88, Pohang, South Korea, June 13 - 17 2010. AIP Conference Proceedings. doi: 10.1063/1.3457640.

[33] C. Agelet de Saracibar, M. Chiumenti, M. Cervera, N. Dialami, D. Santiago, and G. Lombera. Advances in the numerical simulation of 3D FSW processes. In *Proceedings of the International Symposium on Plasticity and its Current Applications, Plasticity 2011*, Puerto Vallarta, Mexico, January 3 - 8 2011.

[34] M. Chiumenti, M. Cervera, C. Agelet de Saracibar, and N. Dialami. Numerical modeling of friction stir welding processes. *Computer Methods in Applied Mechanics and Engineering*, 254:353–369, 2013. doi: 10.1016/j.cma.2012.09.013.

[35] N. Dialami, M. Chiumenti, M. Cervera, and C. Agelet de Saracibar. An apropos kinematic framework for the numerical modelling of friction stir welding. *Computers and Structures*, 117:48–57, 2013. doi: 10.1016/j.compstruc.2012.12.006.

[36] M. Chiumenti, M. Cervera, C. Agelet de Saracibar, and N. Dialami. A novel stress-accurate FE technology for highly non-linear analysis with incompressibility constraint. application to the numerical simulation of the FSW process. In *Proceedings of the International Conference on Numerical Methods in Forming Processes, NUMIFORM*, Shenyang, China, 2013, 2013. AIP Conference Proceedings. (to be published).

[37] M. Cervera, C. Agelet de Saracibar, and M. Chiumenti. Comet – a coupled mechanical and thermal analysis code. data input manual. version 5.0. Technical Report IT-308, CIMNE, Barcelona, Spain, 2002. URL http://www.cimne.com/comet.

[38] C. Agelet de Saracibar, M. Chiumenti, Q. Valverde, and M. Cervera. On the orthogonal subgrid scale pressure stabilization of finite deformation J2 plasticity. *Computer Methods in Applied Mechanics and Engineering*, 195:1224–51, 2006. doi: 10.1016/j.cma.2005.04.007.

[39] M. Cervera, M. Chiumenti, Q. Valverde, and C. Agelet de Saracibar. Mixed linear/linear simplicial elements for incompressible elasticity and plasticity. *Computer Methods in Applied Mechanics and Engineering*, 192:5249–5263, 2003.

[40] M. Chiumenti, Q. Valverde, C. Agelet de Saracibar, and M. Cervera. A stabilized formulation for incompressible plasticity using linear triangles and tetrahedra. *International Journal of Plasticity*, 20:1487–1504, 2004. doi: 10.1016/j.ijplas.2003.11.009.

[41] C. Agelet de Saracibar, M. Cervera, and M. Chiumenti. On the formulation of coupled thermoplastic problems with phase-change. *International Journal of Plasticity*, 15:1–34, 1999.

[42] M. Cervera, C. Agelet de Saracibar, and M. Chiumenti. Thermo-mechanical analysis of industrial solidification processes. *International Journal for Numerical Methods in Engineering*, 46:1575–1591, 1999.

[43] J. Donea, A. Huerta, J.-P. Ponthot, and A. Rodríguez-Ferran. *Encyclopedia of Computational Mechanics*, chapter Arbitrary Lagrangian-Eulerian Methods. John Wiley & Sons, Ltd, 2004. doi: 10.1002/0470091355.ecm009.

[44] R. Boman and J.-P. Ponthot. Efficient ALE mesh management for 3D quasi-eulerian problems. *International Journal for Numerical Methods in Engineering*, 92:857 − 890, 2012. doi: 10.1002/nme.4361.

[45] R. Boman and J.-P. Ponthot. Enhanced ALE data transfer strategy for explicit and implicit thermomechanical simulations of high-speed processes. *International Journal of Impact Engineering*, 53:62–73, 2013. doi: 10.1016/j.ijimpeng.2012.08.007.

[46] P. Bussetta, R. Boman, and J.-P. Ponthot. Novel three-dimensional data transfer operators using auxiliary finite volume mesh or mortar elements and based over numerical integration. *in preparation*.

[47] P. Bussetta and J.-P. Ponthot. A finite volume based data transfer method for remeshing. application to metal forming problems. In *Proceedings of the 18th International Symposium on Plasticity and Its Current Applications*, San Juan, Puerto Rico, January 2012. URL `http://hdl.handle.net/2268/100394`.

[48] J.P. Ponthot. Unified stress update algorithms for the numerical simulation of large deformation elasto-plastic and elasto-viscoplastic processes. *International Journal of Plasticity*, 18:91–126, 2002. doi: 10.1016/S0749-6419(00)00097-8.

[49] C. Agelet de Saracibar, M. Chiumenti, M. Cervera, N. Dialami, and A. Seret. Computational modeling and sub-grid scale stabilization of incompressibility and convection in the numerical simulation of friction stir welding processes. *Archives of Computational Methods in Engineering*, 21(1), 2014.